Coupling of FDM and FEM in seismic wave propagation

Florent de Martin, Hormoz Modaressi, Hideo Aochi

4th International Conference on
Earthquake Geotechnical Engineering
June 25-28, 2007
Paper No. 1743

COUPLING OF FDM AND FEM IN SEISMIC WAVE PROPAGATION

Florent DE MARTIN[1], Hormoz MODARESSI[2], Hideo AOCHI[3]

ABSTRACT

A specific approach is studied to couple two well-known numerical methods, a finite difference method (FDM) and a finite element method (FEM) for simulating regional seismic wave propagation to local site response. This coupling uses a technique of the "paraxial approximation" in order to input in the FEM the seismic wave generated in the FDM. The main advantage of this approach is to locally extract an area of interest where non-linear soil response or complex geometry is important from the regional wave propagation in a relatively simple medium. This result in taking advantage of both methods: the portability of the FDM and the flexibility of the FEM. This paper presents a theoretical framework of the paraxial approximation, through which the coupling is realized between the FDM and the FEM, and demonstrates some examples for the validation of the proposed coupling technique as well as its possible applications.

Keywords: coupling, finite difference, finite element, paraxial approximation, site effects.

INTRODUCTION

In order to quantitatively study soil responses under any seismic excitation, one has to describe the spatio-temporal evolution of the incident seismic wave field so that a seismic source should be integrated in the model volume (e.g., Bouchon, 1979). This may be principally possible in any method; however, it is still extremely burdensome from a computational point of view, especially if the source-site distance is much longer than the scale of the studied site. Thus it is always worthwhile separating technically the different aspects of incident waves and local site responses, for which the mathematical and physical consistence is required (e.g. domain reduction methods, Bielak et al., 1999; Yoshimura et al., 1999). Such a coupling can give the advantages such as a gain of time compared to the execution of the whole simulation, and a good assessment of site condition for the parameter study.

In this study, we have two different methods. Finite Difference Methods (FDM) are often adopted for simulating the seismic wave propagation from an excited source in a large volume, mostly because the mathematical formulation and grid structure are handy and easy to implement for a parallel computing. Regardless of the inevitable numerical dispersion, they can provide a satisfying result at low frequency in a medium of relatively weak material heterogeneity. On the other hand, local site responses are often studied using Finite Element Methods (FEM), because of the necessity of treating a geometrically complex medium with possible non-linear and multiphase behaviour. This flexibility, in contrast, makes difficult to compute a large volume. The purpose of this paper is to make use of the

[1] Civil Engineer, Development Planning and Naturals Risks Division, BRGM, France, Email: f.demartin@brgm.fr
[2] Professor, Development Planning and Naturals Risks Division, BRGM, France, Email: h.modaressi@brgm.fr
[3] Researcher, Development Planning and Naturals Risks Division, BRGM, France, Email: h.aochi@brgm.fr

merits of such two methods and couple them reasonably in mathematical and physical frameworks. The coupling is carried via "paraxial elements" (or parabolic elements) implemented in the FEM. First we will show the theoretical description. Then this technique will be tested comparing to the results entirely simulated by the FDM. At last, some examples of local topography and local basin effects will be demonstrated.

FORMULATION OF PARAXIAL APPROXIMATION

In this section, we give the mathematical formulation of the paraxial approximation in the FEM code (GEFDYN), which has been developed for geomechanical applications since Modaressi (1987).

History of the paraxial approximation

The paraxial or parabolic approximation (or 15° approximation) was presented for the first time by (e.g. Claerbout, 1976) for scalar waves, then completed and studied in detail for elastic waves (e.g. Engquist and Majda, 1977; Clayton and Engquist, 1977). This approximation is useful for the computation in the transient domain and permits to build dynamic impedance, locally in space and in time, on the interface Σ (Figure 1). Cohen and Jennings (1983) proposed a numerical procedure of this approximation in the finite element methods. It should be noted that the domains $\Omega_{s'}$ and Ω_s surrounding the interface Σ are supposed to be elastic whereas the domain Ω_x could be inelastic (the paraxial approximation has also been developed for heterogeneous or nonlinear medium (Bamberger *et al*., 1986)). Basically, the paraxial approximation is used to absorb the outgoing waves, avoiding any artificial reflection on the interface; however, it is possible to use this approximation for both introducing physical signals for the inside Ω_s and absorbing unnecessary outgoing waves from Ω_s to $\Omega_{s'}$ via Σ (e.g. Modaressi, 1987; Aubert, 1997).

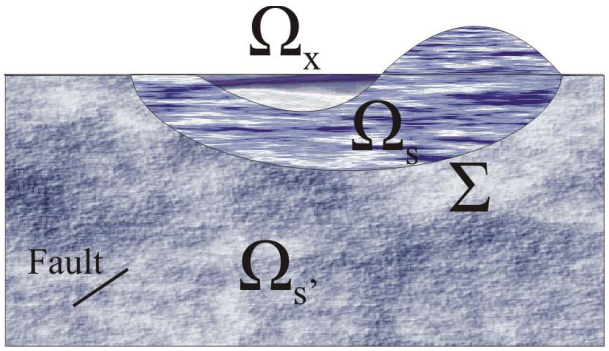

Figure 1. Schematic illustration of the problem. Seismic waves are generated on earthquake faults in an elastic domain $\Omega_{s'}$. The volume of interest consists of an elastic domain Ω_s and an (in)elastic domain Ω_x, extracted along the interface Σ.

Definition of spectral impedance of the interface Σ

The spectral impedance $\hat{\underline{\tau}}$ represents, in the Fourier domain, the action imposed by the exterior domain $\Omega_{s'}$ on the interior domain Ω_s. In order to derive the paraxial approximation, the equation of motion in an elastic medium:

$$(\lambda + \mu)\underline{grad}\,(div\,\underline{u}) + \mu\Delta\underline{u} - \rho\partial_{tt}^{2}\underline{u} = 0 \qquad \text{(Eq. 1)}$$

shall be projected on a local plane $\underline{x}'$ formed by $(\underline{e}_1', \underline{e}_2')$ and on the axis $\underline{e}_3$ (Figure 2). Here λ and μ are the Lame coefficients and $\underline{u}$ is the displacement vector which verify the equation of motion. With respect to the projected one of Eq (1), the solutions in the Fourier domain, $\hat{\underline{u}}'$ and $\hat{u}_3$, permit to derive the spectral impedance on the interface Σ :

$$\underline{\hat{\tau}}\left(\underline{\xi}^{'}, x_3 = 0, \omega\right) = a_0\,\underline{e}_3 + b_0\,\underline{\xi}^{'} + c_0\,\underline{\xi}^{'} \wedge \underline{e}_3 \qquad \text{(Eq. 2)}$$

where $\underline{\xi}^{'}$ is the wave vector associated with the plane $\underline{x}^{'}$ formed by $\left(\underline{e}_1^{'}, \underline{e}_2^{'}\right)$, and a_0, b_0 and c_0 are functions of $\left|\underline{\xi}^{'}\right|$, ω (the pulsation), $\underline{\hat{u}}'(x_3 = 0)$, $\hat{u}_3(x_3 = 0)$, $\xi_s^{\,2} = \dfrac{\omega^2}{V_s} - \left|\underline{\xi}^{'}\right|^2$ and $\xi_p^{\,2} = \dfrac{\omega^2}{V_p} - \left|\underline{\xi}^{'}\right|^2$.

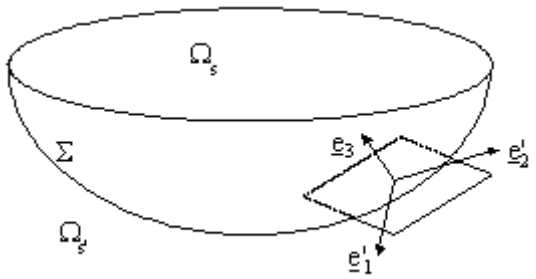

Figure 2. Reference system. The coordinate $(\underline{e}_1', \underline{e}_2', \underline{e}_3)$ is locally defined on the interface Σ. $\underline{e}_3$ is the normal vector pointing inside the domain Ω_s, and $\left(\underline{e}_1^{'}, \underline{e}_2^{'}\right)$ forms the tangential plane $\underline{x}^{'}$.

Paraxial approximation of the impedance

The spectral impedance (Eq. 2) can be written in the physical domain through the Fourier inverse transform:

$$\underline{\tau}\left(\underline{x}', x_3 = 0, t\right) = \frac{1}{\sqrt{2\pi}} \int_{-\infty}^{+\infty}\int_{-\infty}^{+\infty} \underline{\hat{\tau}}\left(\underline{\xi}^{'}, x_3 = 0, \omega\right) \exp\left[-i\left(\omega t + \left(\underline{\xi}^{'}.\underline{x}'\right)\right)\right] \partial\omega\,\partial\underline{\xi}^{'} \,. \qquad \text{(Eq. 3)}$$

However, this integration cannot be evaluated theoretically. Engquist and Majda (1977) proposed to develop the wave numbers ξ_s and ξ_p in the functions of the ratio κ:

$$\begin{cases} \xi_s = \dfrac{\omega}{V_s}\left(1 - V_s^{\,2}\kappa^2\right)^{1/2} \\ \xi_p = \dfrac{\omega}{V_p}\left(1 - V_p^{\,2}\kappa^2\right)^{1/2} \end{cases} \qquad \text{with} \qquad \kappa = \frac{\left|\underline{\xi}^{'}\right|}{\omega} \,. \qquad \text{(Eq. 4)}$$

The paraxial approximation is based on the assumption that κ is small enough compared to the unity so that we can use only the lower orders of the following Taylor development:

$$\xi_\alpha = \frac{\omega}{V_\alpha}\left(1 - V_\alpha^{\,2}\kappa^2\right)^{1/2} \approx \frac{\omega}{V_\alpha}\left[1 - \frac{1}{2}V_\alpha^{\,2}\kappa^2 + \ldots\right] \qquad \text{with} \quad \alpha = s, p \,. \qquad \text{(Eq. 5)}$$

The figure 3 illustrates the exact solution and the approximations. These approximations are correct when the norm of the wave vector $\underline{\xi}^{'}$ is small (i.e. the waves are propagating in a direction close to $\underline{e}_3$). This will explain in the later demonstration how the domain shape Σ is important with respect to the location of seismic source (i.e. incident wave direction).

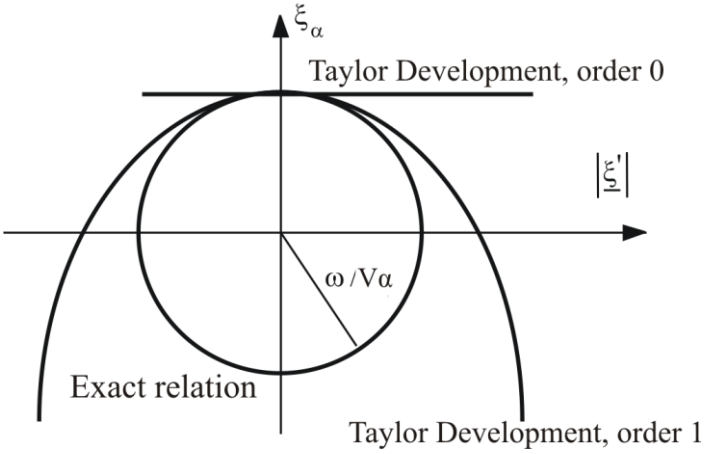

Figure 3. $\xi_\alpha = f\left(\left|\underline{\xi}'\right|\right)$ **: Exact solution and Taylor development (order 0 and 1)**

In this study, we use the zero-order paraxial approximation. It should be noted that the paraxial approximation of order one does not improve significantly the results and that high order approximations fetch up to instabilities (e.g. Clayton and Engquist, 1977). As a result, the spectral impedance, Eq. 2, will be simplified in the following:

$$\hat{\underline{\tau}}\left(\underline{\xi}', x_3 = 0, \omega\right) = -i\omega\rho\left(V_p \hat{u}_3\left(x_3 = 0\right)\underline{e}_3 + V_s \hat{\underline{u}}'\left(x_3 = 0\right)\right), \qquad \text{(Eq. 6)}$$

and the spectral action, Eq. 3 will be written as

$$\underline{\tau}\left(\underline{x}', x_3 = 0, t\right) = -\rho V_p \partial_t u_3\left(x_3 = 0\right)\underline{e}_3 - \rho V_s \partial_t \underline{u}'\left(x_3 = 0\right). \qquad \text{(Eq. 7)}$$

For the simplicity, Eq 7 is further written in the form $\underline{\tau}\left(\underline{x}', x_3 = 0, t\right) = A_0\left(\partial_t \underline{u}\right)$.

Variational formulation

Across the interface Σ between $\Omega_{s'}$ and Ω_s, the continuity of the displacement and of the stress vector is required:

$$\begin{cases} \underline{u}_s + \underline{u}_{s'} = 0 \\ \underline{\tau}_s + \underline{\tau}_{s'}\left(\underline{u}_{s'}\right) = 0 \end{cases} \qquad \text{(Eq. 8)}$$

Let us decompose the total field $\underline{u}_{s'}$ on the interface Σ into an incident wave field $\underline{u}_{i'}$ and a diffraction-radian field $\underline{u}_{r'}$:

$$\underline{u}_{s'} = u_{i'} + u_{r'}. \qquad \text{(Eq. 9)}$$

Supposing the neighborhood of the interface Σ homogenously linear and the diffraction-radian field $\underline{u}_{r'}$ ruled by the paraxial approximation, we can derive after Eqs 7, 8 and 9 the zero-order approximation:

$$\underline{\tau}_s = -\underline{\tau}_{s'}\left(\underline{u}_{s'}\right) = -\underline{\tau}_{s'}\left(\underline{u}_{i'}\right) - \underline{\tau}_{s'}\left(\underline{u}_{r'}\right) \approx -\underline{\tau}_{s'}\left(\underline{u}_{i'}\right) - A_0\left(\partial_t \underline{u}_{r'}\right) = -\underline{\tau}_{s'}\left(\underline{u}_{i'}\right) - A_0\left(\partial_t \underline{u}_{s'}\right) + A_0\left(\partial_t \underline{u}_{i'}\right). \qquad \text{(Eq. 10)}$$

This relation gives the evolution law of the stress vector on the interface Σ. A_0 is the paraxial operator defined above that models approximately the stress vector within a medium where waves are propagating in one direction. For the purpose of the coupling, the stress field expressed by $\underline{\tau}_{s'}(\underline{u}_{i'})$ and the incoming wave velocity field $A_0(\partial_t \underline{u}_{i'})$ are required. By injecting the developed form of $\underline{\tau}_s$ in the virtual work principle, we can derive the specific equation in our formulation:

$$\int_{\Omega_s} \rho \partial_{tt} \underline{u}_{s'} \cdot \underline{w} d\Omega + \int_{\Omega_s} \underline{\underline{\sigma}}_{s'} : \underline{\underline{\varepsilon}}(\underline{w}) d\Omega + \int_{\Sigma} A_0(\partial_t \underline{u}_{s'}) \cdot \underline{w} d\Sigma = \int_{\Omega_s} \rho \underline{g} \cdot \underline{w} d\Omega + \int_{\Sigma} (-\underline{\tau}_{s'}(\underline{u}_{i'}) + A_0(\partial_t \underline{u}_{i'})) \cdot \underline{w} d\Sigma$$

(Eq. 11)

VALIDATION OF THE COUPLING

As a preliminary study, we have tested a plane incident wave and confirmed the validity of our coupling procedure. In this paper, another validation test (seismic wave propagation) is shown.

Model setting

In order to test our coupling procedure, we set up a semi-infinite homogenous elastic medium in 2D (V_s = 1500 m.s^{-1}, V_p = 3200 m.s^{-1} and ρ = 2280 kg.m^{-3} in all the domains $\Omega_{s'}$, Ω_s and Ω_x). Note that the domain Ω_x does not exist practically but is included in the domain Ω_s. A FDM with the 2nd order staggered grid is used (Virieux and Madariaga, 1982) for modeling the seismic source in the domain $\Omega_{s'}$ and the radiated wave propagation to the domains Ω_s and Ω_x across Σ (Figure 4). The seismic source is characterized by giving a seismic moment tensor, namely, magnitude, fault's orientation and slip direction, which is incorporated as a double couple force in the equation of motion. In Figure 4, fault orientation is taken to be 45° clockwise from the Y axis and fault slip is parallel to it. The source duration is assumed to be 0.02 seconds (=50Hz). As the FDM grids and the FEM nodes are not always situated at the same coordinates, a linear interpolation is adopted in the FDM code for each component of the velocity and the stress fields on the interface Σ (110 points on the curve in Figure 4). For the simplicity and for avoiding unexpected scaling problem, the time step of the FDM is the same as the FEM (0.0002 second) and grid (element) spacing is 2 m, the same scale as the FEM.

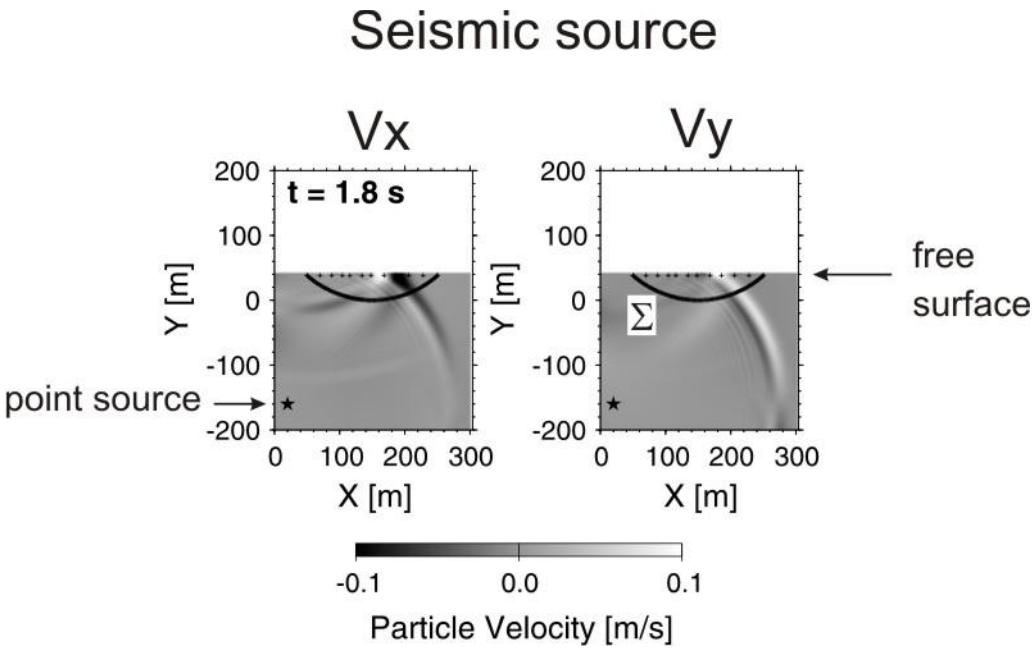

Figure 4. Snapshot of simulated wave propagation from a source to site using a finite difference method. The panel shows each component of velocity field. Black points represent the output points for the FEM simulation (110 points on the curve Σ, and 9 points on the free surface for

comparison). Seismic source is implemented at (x, y) = (20 m, -160 m) with the existence of the free ground surface at y=38 m. The P and S waves propagate from the source.

Inside the domain Ω_s, wave propagation is calculated in the FEM through the interface Σ (Figure 5). Now that the medium is elastic and homogeneous without any complexity on the whole domainsΩ_s, and Ω_s, the simulation results of wave propagation coupled in the FEM in the domain Ω_s should give the identical results calculated directly by the FDM. In order to evaluate the quality of our approach, we compared the synthetic velocity on several points located on the free surface (See Figures 4 and 5). Figure 5 shows in one hand the node's numbers where the velocity computed by the FDM and by the FEM are compared and in other hand the mesh of the FEM. We plotted for each method the two component of the velocity at some location (Fig. 6).

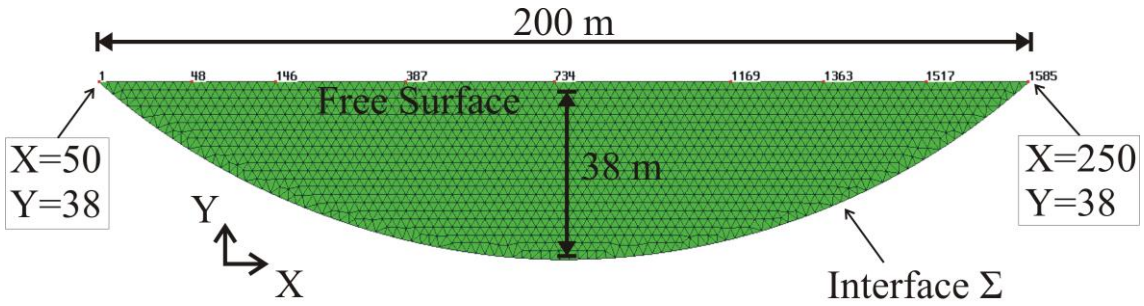

Figure 5. FEM mesh for calculating the domain Ω_s. The node's numbers are 1, 48 (not used), 146, 387, 734, 1169 (not used), 1363, 1517 (not used) and 1585 from left to right, located on the free surface, corresponding to the black marks in Figure 4.

Simulation result

Figure 6 compares each component of the velocity at six stations illustrated in Figures 4 and 5. It is observed that the coupled simulation in the FEM gives the correct wave propagation (arrivals of the P and S waves and their phases and amplitudes). The oscillations appearing just after the arrival of the S-wave originate from the seismic source implementation in the FDM (the source duration is not enough long with respect to the grid spacing). However it is surprising that such a wave correctly propagates in the coupling simulation. In detail, some misfit, especially for the S wave appears slightly at nodes 1363 and 1585, which are far ends from the seismic source location. For such points (on the right hand side of the domain Ω_s when the seismic waves arrives from the left hand side), the incident angle of the incoming wave becomes low on the interface Σ. Thus the paraxial approximation may not work correctly enough.

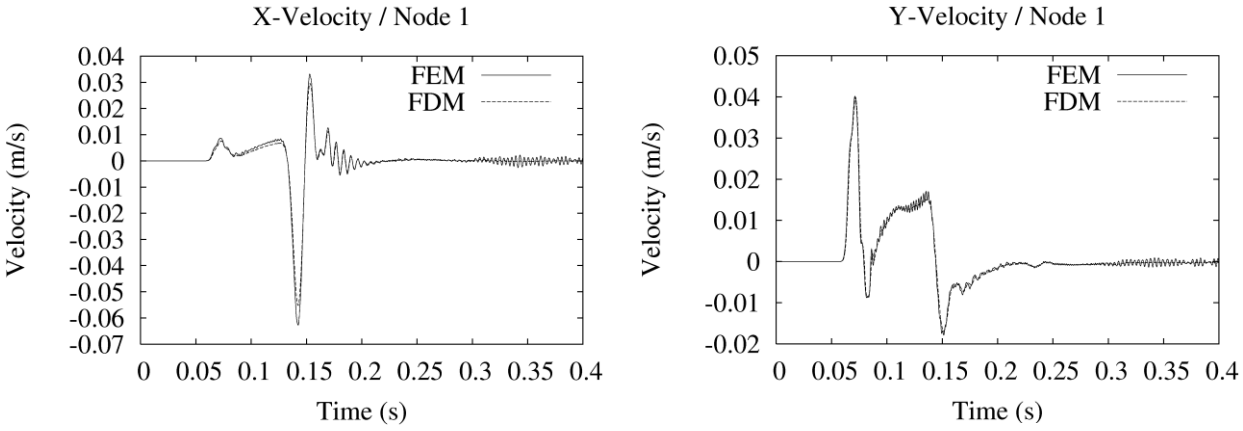

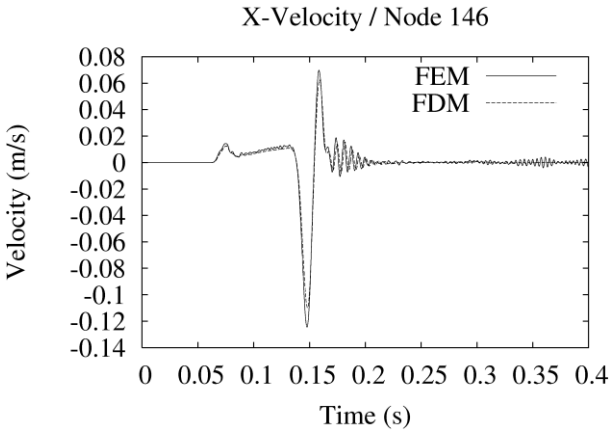
X-Velocity / Node 146
Velocity (m/s)
Time (s)
FEM
FDM

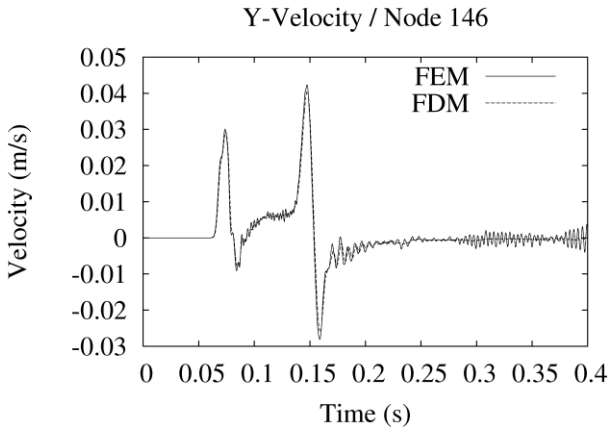
Y-Velocity / Node 146
Velocity (m/s)
Time (s)
FEM
FDM

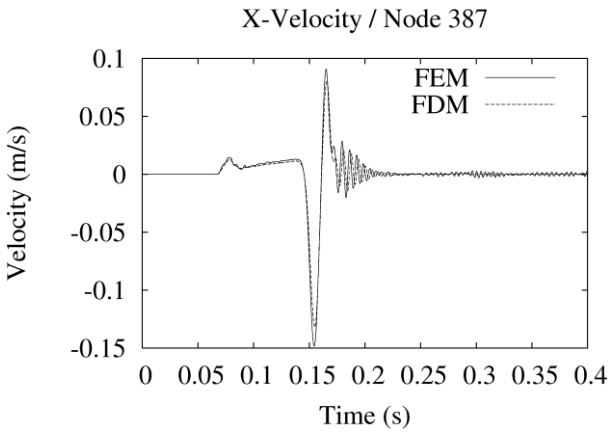
X-Velocity / Node 387
Velocity (m/s)
Time (s)
FEM
FDM

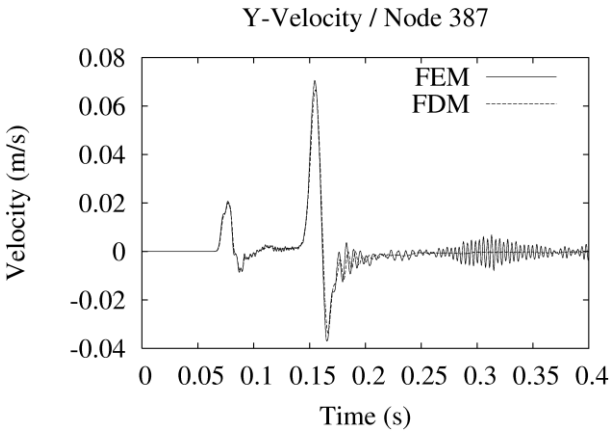
Y-Velocity / Node 387
Velocity (m/s)
Time (s)
FEM
FDM

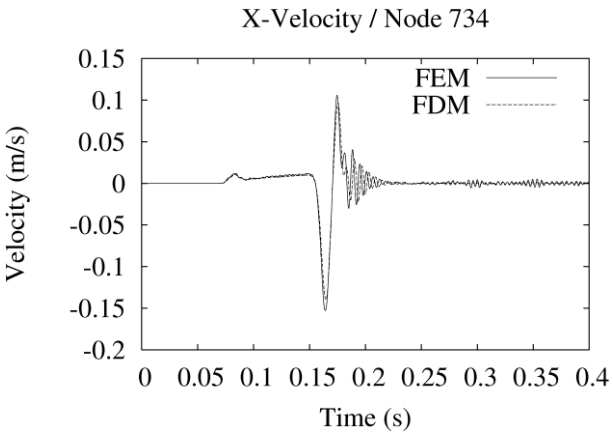
X-Velocity / Node 734
Velocity (m/s)
Time (s)
FEM
FDM

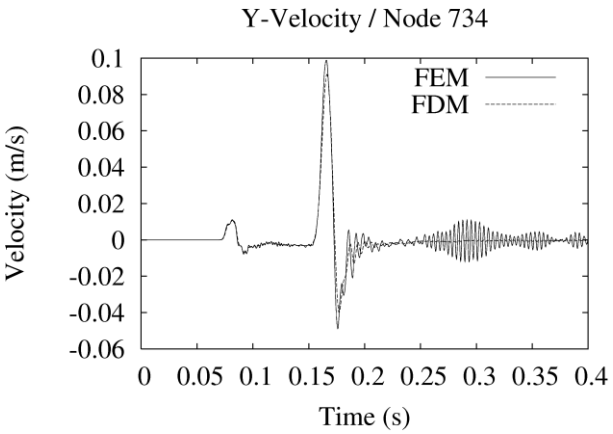
Y-Velocity / Node 734
Velocity (m/s)
Time (s)
FEM
FDM

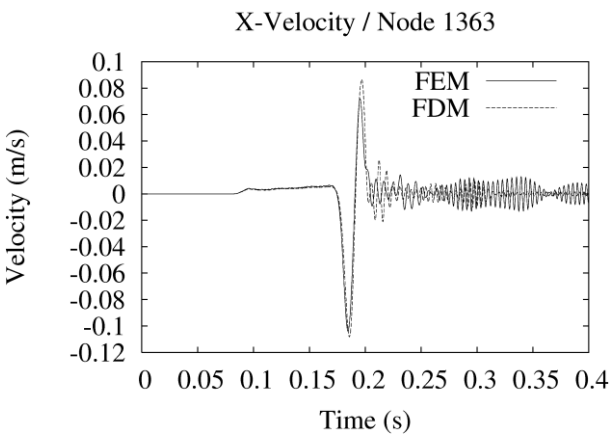
X-Velocity / Node 1363
Velocity (m/s)
Time (s)
FEM
FDM

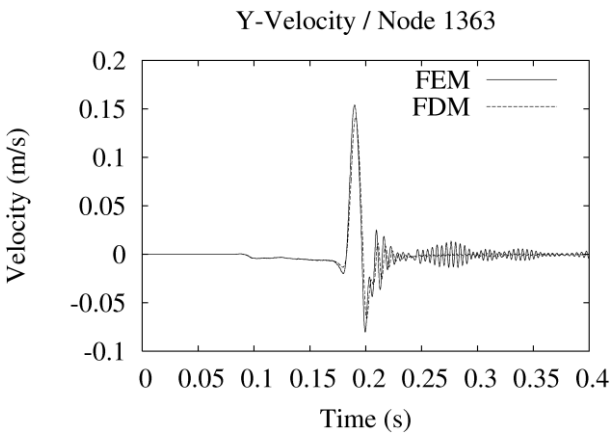
Y-Velocity / Node 1363
Velocity (m/s)
Time (s)
FEM
FDM

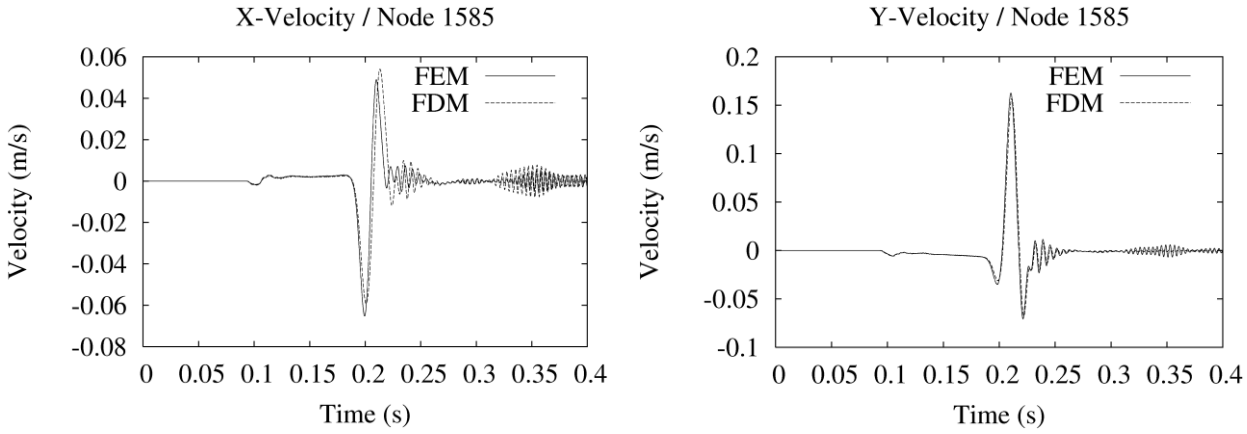

Figure 6. Comparison of synthetic velocity in each component at six points on the free surface (see Figures 4 and 5). No filter is applied on both the FEM and FDM simulations.

After the passage of the body waves, spurious oscillations appear. This can be mainly due to the wave multi-reflection in the domain Ω_s. The zero-order approximation we use in this study may not be able to absorb the wave perfectly. Nevertheless, the amplitude of these perturbations is small compared to the main wave (ratio 6%). Some improvement would be expected by using a higher order of the paraxial approximation. For practical uses, however, Figure 6 confirms that implemented paraxial elements behave like a transparent boundary good enough to couple the two domains for the wave propagation.

APPLICATIONS FOR SITE EFFECT STUDY

In order to show the example of the site effect study, we change the property of the medium in the domain Ω_s. Considering that such local heterogeneity should not affect the global wave propagation in the domain $\Omega_{s'}$, we are able to use the same incident waves on the interface geometry Σ without recalculating other configuration using the FDM. Thus we keep the same interface geometry Σ as well as the same linear elastic properties around the interface Σ (V_s, V_p and ρ).

First Figure 7 shows the reference homogenous model (identical to the result shown in Figure 6). Six others local configurations are demonstrated from Figures 8 to 13. In Figure 8, 9 and 10, the effects of local topography with complex geometry are modeled and in Figures 11, 12 and 13 the basin effects are simulated by introducing the material heterogeneity. We do not aim at discussing quantitatively each simulation result in this paper. The objective of this paper is to show the potential capacity of such coupled simulations.

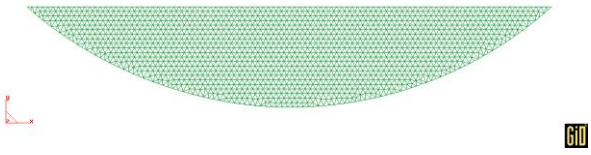

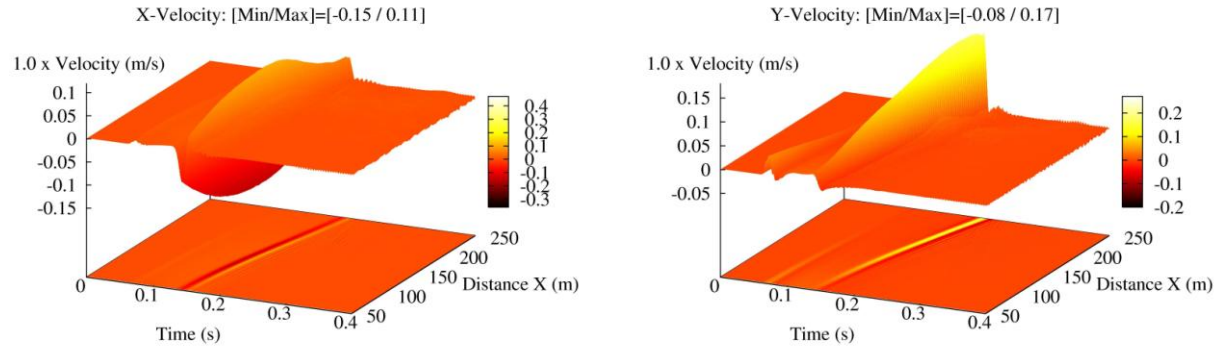

Figure 7. Reference domain. Top: Model geometry and meshing. Bottom: Synthetic seismograms at each points along the free surface (x and y components, respectively).

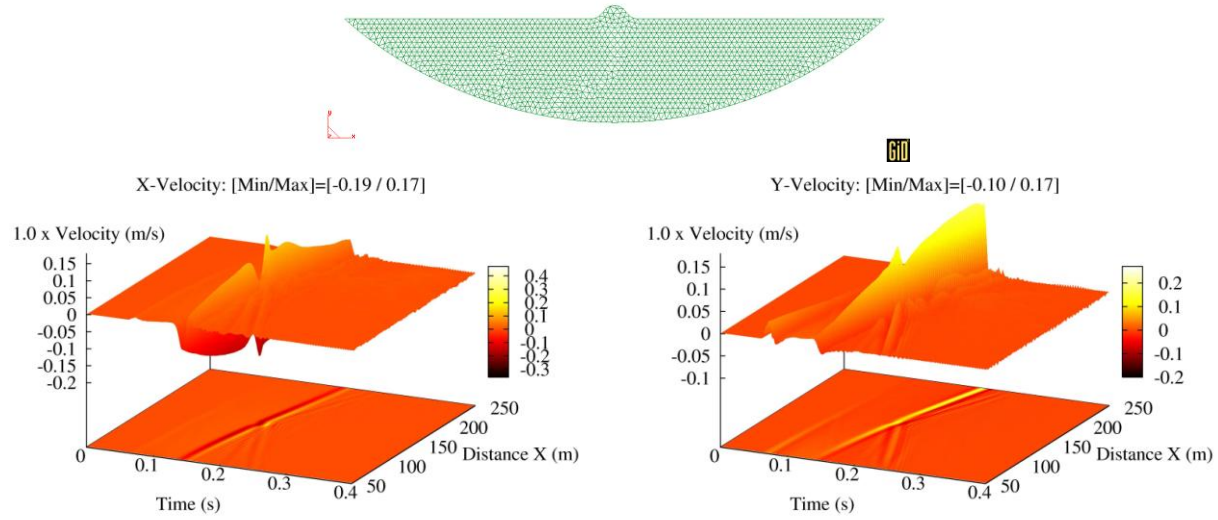

Figure 8. Effect of a hill smaller than the wavelength of the input wave

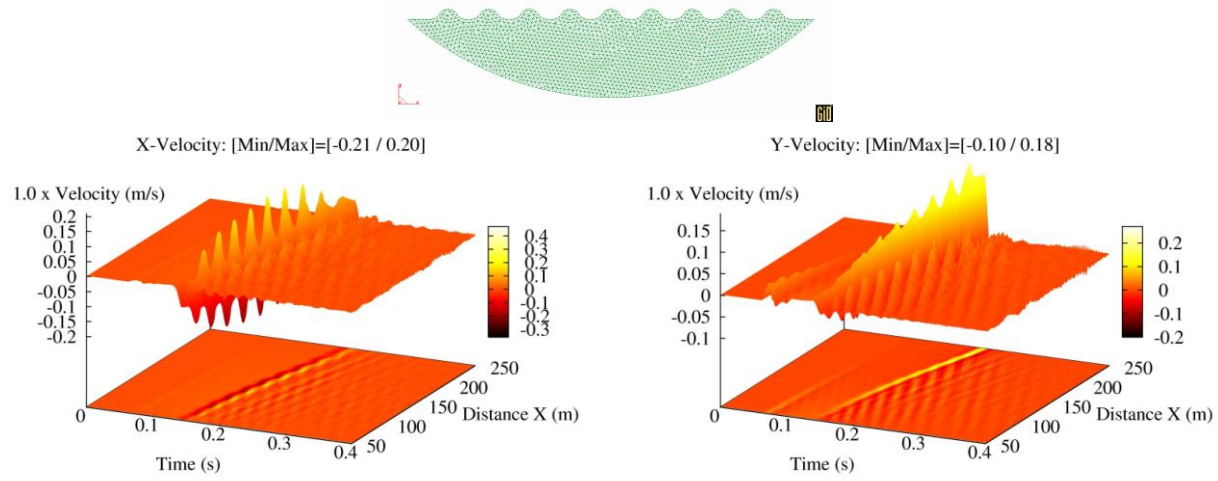

Figure 9. Effect of a set of hills smaller than the wavelength of the input wave

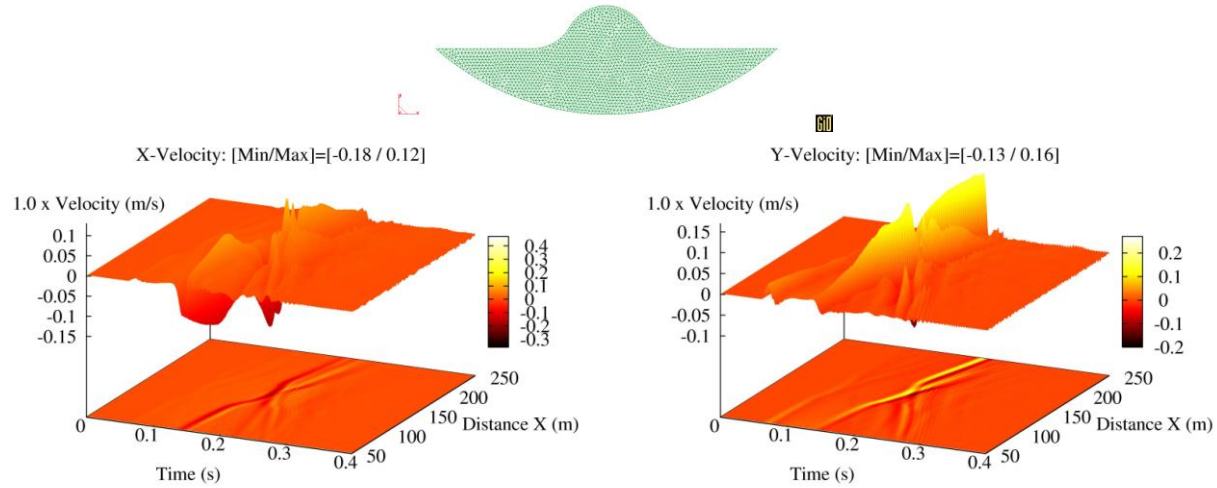

Figure 10. Effect of a hill larger than the wavelength of the input wave

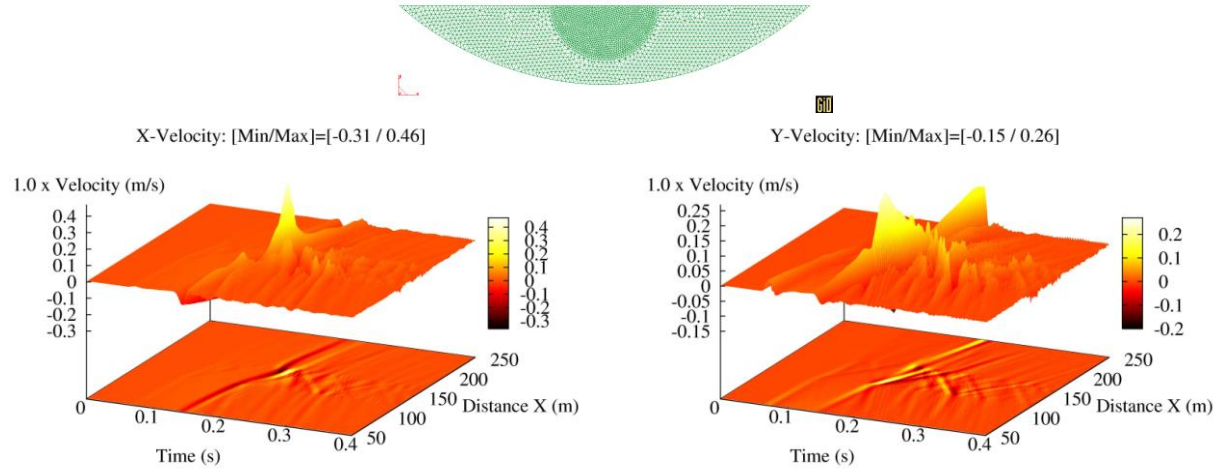

Figure 11. Site effect: the properties of the domain Ω_x are Vs=750 m.s^{-1}, Vp=1490 m.s^{-1} and ρ=2000 kg.m^{-3}. The shape of the domain Ω_x is a half-circle with a diameter of 50 m

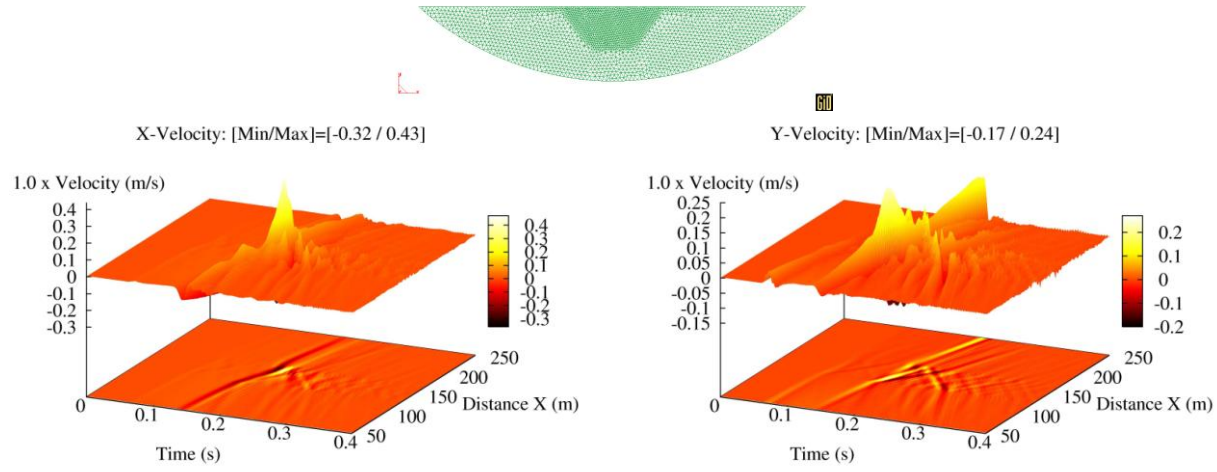

Figure 12. Site effect: the properties of the domain Ω_x are Vs=750 m.s^{-1}, Vp=1490 m.s^{-1} and ρ=2000 kg.m^{-3}. The shape of the domain Ω_x is a trapeze with a base of 50 m

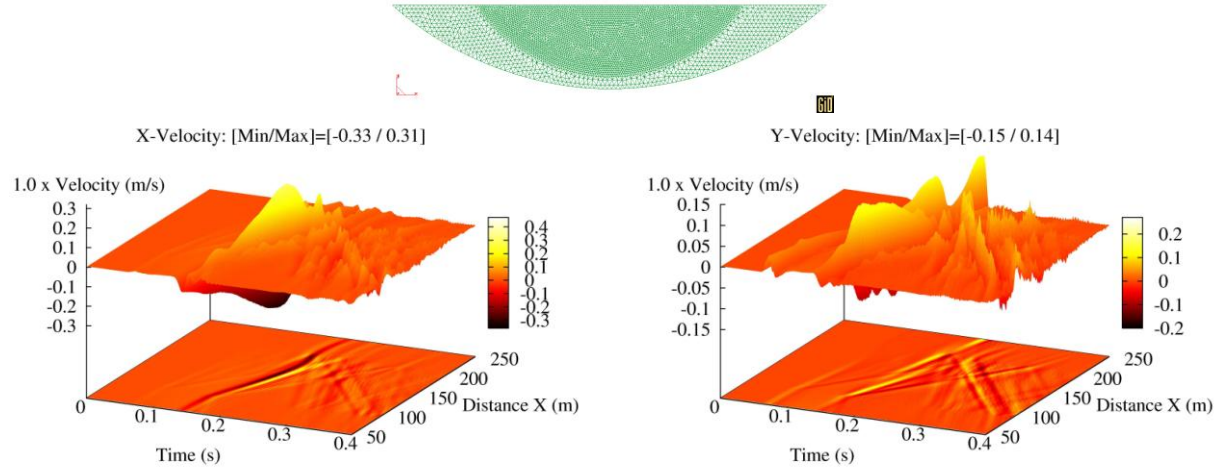

Figure 13. Site effect: the properties of the domain Ω_x are Vs=750 m.s^{-1}, Vp=1490 m.s^{-1} and ρ=2000 kg.m^{-3}. The shape of the domain Ω_x is the bottom of a circle with a diameter of 150 m

DISCUSSION

Further works are ongoing in order to assess the sensitivity of the coupling by studying the influence of the coarseness of the finite difference method's grid. It seems also important to evaluate the gain of accuracy obtained if the paraxial elements were used with an approximation of order one. Eventually, with the current development of the boreholes and by making some assumptions on the wave propagation, the paraxial approximation could be used to input natural seismograms on the interface Σ in order to test the accuracy of the finite element method to assess site effects on nonlinear soils.

CONCLUSION

This paper demonstrates the coupling simulation of seismic wave propagation from the FDM to the FEM. The coupling is carried out through the paraxial approximation developed in the FEM code. The main step of the theoretical formulation is first shown and then several examples are demonstrated. After the preliminary tests in a homogeneous elastic medium, it is found that such coupling works correctly and that we can handily get the expected results. It is proposed that this kind of coupling simulation is very useful for further local site effect, taking into account of the source and path effects. This will allow us to evaluate more quantitatively the local site effect for seismic hazard analysis.

ACKNOWLEDGEMENT

This work is carried out in the framework of BRGM research program on "Seismic Risk Study". This is also a contribution to the French National Research (ANR) programs, SEISMULATOR (seismic simulation in complex source-site context, 2006-2008) and NUMASIS (Adaptation et Optimisation des Performances Applicatives sur architectures NUMA. Étude et Mise en Oeuvre sur des Applications en SISmologie, 2006-2008).

REFERENCES

Aubert, P., Méthodes Meshless en Géomécanique. Thèse de doctorat de l'Ecole Centrale Paris, France, 1997.

Bamberger, A., Enquist, B., Halpern, L., Joly, P. Higher order paraxial wave equation approximations in heterogeneous media. INRIA, research report N°558, 1986.

Bielak, J., Loukakis, K., Hisada, Y., Yoshimura, C. Domain Reduction Method for Three-Dimensional Earthquake Modeling in Localized Regions, Part I: Theory. Bull. Seism. Soc. Am., Vol. 93, No. 2, pp. 817-824, 2003.

Bouchon, M. Predictability of ground displacement and velocity near an earthquake fault – An example: the Parkfield earthquake of 1966. J. Geophys. Res. Vol 84, pp. 6149-6156, 1979.

Claerbout, J.F. Fundamentals of geophysical Data Processing. McGraw-Hill Inc, 1976.

Clayton, R. and Enquist, B. Absorbing boundary conditions for acoustic and elastic wave equations. Bull.. Seism. Soc. Am., Vol 67, No 6, pp. 1529-1540, 1977.

Cohen, M., and Jennings, P.C. Silent boundarymethods for transient analysis. Computational Methods for Transient Analysis (Ed. Belytschko, Hugues), Elsevier Science Publishers, 1983.

Enquist, B. and Majda, A. Absorbing boundary conditions for the numerical simulation of waves. Mathematics of Computation, vol, 31, n°139, pp. 629-651, 1977.

Modaressi, H. Modélisation numérique de la propagation des ondes dans les milieux poreux anélastiques. PhD Thesis, Ecole Centrale Paris, France, 1987.

Virieux, J. and Madariaga, R., Dynamic faulting studied by a finite difference method, Bull. Seismo. Soc. Am., Vol. 72, pp. 345-269, 1982.

Yoshimura, C., Bielak, J., Hisada, Y., Fernandez, A. Domain Reduction Method for Three-Dimensional Earthquake Modeling in Localized Regions, Part II: Verification and Applications. Bull. Seism. Soc. Am., Vol. 93, No. 2, pp. 825-840, 2003.